Lumped Parameter Hemodynamic modelling and ODEs-for Upper Thoracic aorta

Adisu Mengesha Assefa [1,2,3]
[1]Erasmus Mundus Joint Master in Biomedical Engineering (EMMBIOME) Scholar
[2]University of Patras, 26504, Patras, Greece
[3]Email: adisumengesha315@gmail.com | adisu.mengesha@upatras.gr

A B S T R A C T

I developed and analyzed a 0D lumped-parameter model of the upper thoracic aorta to simulate hemodynamic behavior under various conditions, including bifurcation scenarios. In this work, I coupled a vessel model with a Windkessel terminal model and solved the governing system of ODEs using the forward Euler method. I also performed a comprehensive time step analysis using both machine learning and manual tuning, which allowed me to identify an optimal balance between computational efficiency and solution precision. For model calibration, I employed synthetic data to estimate critical parameters, particularly vascular resistance (R_0) and wall compliance (C_0), and conducted an identifiability analysis. This analysis revealed that while compliance was well constrained, resistance exhibited a higher degree of uncertainty. In the bifurcation analysis, I implemented an iterative Newton–Raphson scheme at each time step to enforce coupling conditions at the bifurcation node. The simulation results confirmed that both mass and energy were conserved, with computed pressures and flow rates aligning closely with physiological expectations. This study highlights the importance of robust numerical methods and careful calibration in achieving realistic hemodynamic simulations.

1.0 Introduction

Hemodynamic modeling is an essential approach to understanding blood flow dynamics in the cardiovascular system. This report presents the implementation and analysis of a zero-dimensional (0D) lumped-parameter blood flow model in a vessel coupled with a Windkessel (WK) terminal model. The primary goal is to solve the system of ordinary differential equations (ODEs) governing the dynamics using the forward Euler method, analyze the effect of different step sizes, and explore the impact of varying wall compliance.

The governing equations for the 0D vessel model, (Formaggia et al., 2010; Quarteroni et al., 2016).

Equation (1):

$$\frac{dV}{dt} = Q_{in}(t) - Q(t)$$

$$\frac{dQ(t)}{dt} = \frac{P(t) - R_0 Q(t) - P_{out}(t)}{L_0}$$

Equation (2):

$$P(t) = P_0 - \frac{V(t) - V_0}{C_0}$$

The vessel is coupled to the WK model with the equations (3):

$$\frac{d}{dt}P_{wk}(t) = \frac{Q_{wk,in}(t) - Q_{wk(t)}}{C_{wk}}$$

$$Q_{wk}(t) = \frac{P_{wk}(t) - P_{ven}}{R^d_{wk}}$$

where the coupling conditions are:

Equation (4):

$$Q_{wk,in}(t) = Q(t),$$

$$P_{out}(t) = P_{wk}(t) + R^p_{wk}, Q(t)$$

where $P_{wk}(t)$and $Q_{wk}(t)$ are pressure and flow rate in the WK element; the parameters C_{wk}, R^p_{wk} and R^d_{wk} represent the terminal compliance, proximal and distal terminal resistances, respectively; P_{ven} is a constant pressure distal to the WK model. Here considered an upper thoracic aorta model, where the thoracic aorta from the aortic root to the descending aorta is simulated as a single 0D vessel model (1)-(2) coupled to a lumped-parameter WK model (3) via relations (4), where the Windkessel model represents the rest of the downstream systemic circulation. Parameters R_0 , L_0 and C_0 are defined as follows (Milišić and Quarteroni, 2010).

$$R_0 = \frac{8\mu L}{\pi r_0^4} \quad L_0 = \frac{\rho L}{\pi r_0^2} \quad C_0 = \frac{3}{2}\frac{\pi r_0^3 L}{E h_0}$$

All model parameters are listed in Table 1 of the supplementary material. The inflow condition $Q_{in}(t)$ to be imposed at the inlet of the vessel is a periodic function of period T = 0.955 s and provided in the Supplementary Material (file "inflow.txt"). As a consequence, the model admits a periodic solution of period T.

1.1 Numerical Scheme

The forward Euler method is employed to solve the system of ODEs. The discretized equations for numerical integration are:

$$V_{n+1} = V_n + \Delta t\left(Q_{in,n} - Q_n\right)$$

$$Q_{n+1} = Q_n + \Delta t\left(\frac{P_n - R_0 Q_n - P_{out,n}}{L_0}\right)$$

Step Size Selection: A machine learning model was used to determine an optimal time step based on accuracy, computational efficiency, and stability. The ML model was trained on simulation data using different time steps, evaluating pressure and flow errors relative to a high-resolution reference solution. The selected time step, 0.006866s, was chosen as it achieved a balance between accuracy and computational cost, minimizing a combined error metric of 0.119775. Feature importance analysis revealed that flow RMSE (53.57%) and computation time (46.43%) were the most influential factors in selecting the optimal time step. After obtaining the ML-selected time step, a manual analysis was performed by selecting additional time steps manually selected values included to compare errors and computation time:

dt_values = *[0.01, 0.005, 0.003, 0.002, 0.006866, 0.001, 0.0005, 0.0001]*

This allowed for a refined evaluation of numerical stability, accuracy, and efficiency.

1.3 Model Simulation and Step Size Analysis

The simulation was run for multiple periods to ensure periodic steady-state convergence. Various step sizes were tested, and it was observed that larger step sizes led to numerical instability, while smaller values provided smooth solutions. The ML-selected provided an optimal balance between stability and computational efficiency.

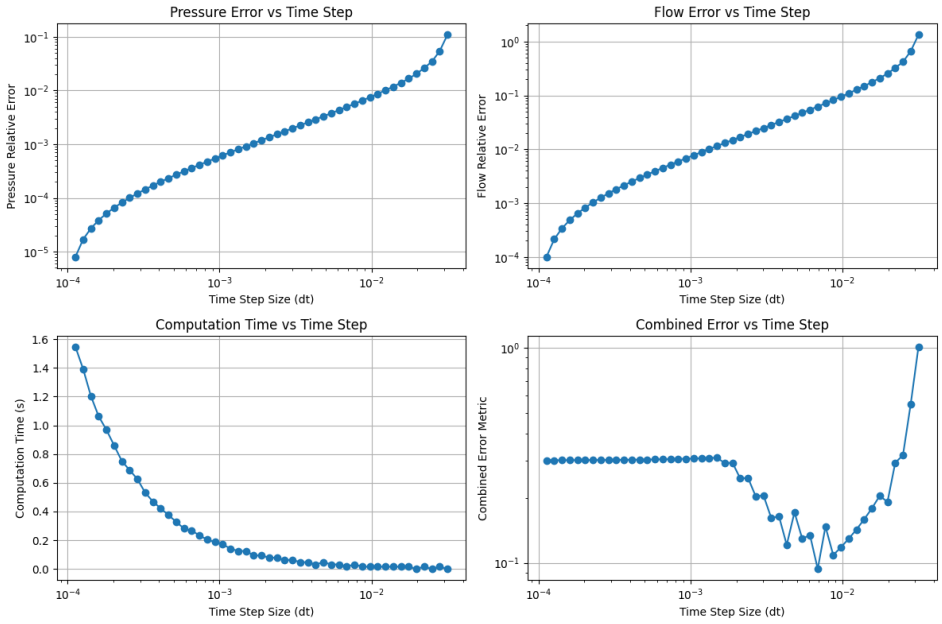

Figure 1: presents the results of time step analysis, illustrating the relationship between time step size and errors in pressure, flow, computation time, and a combined error metric.

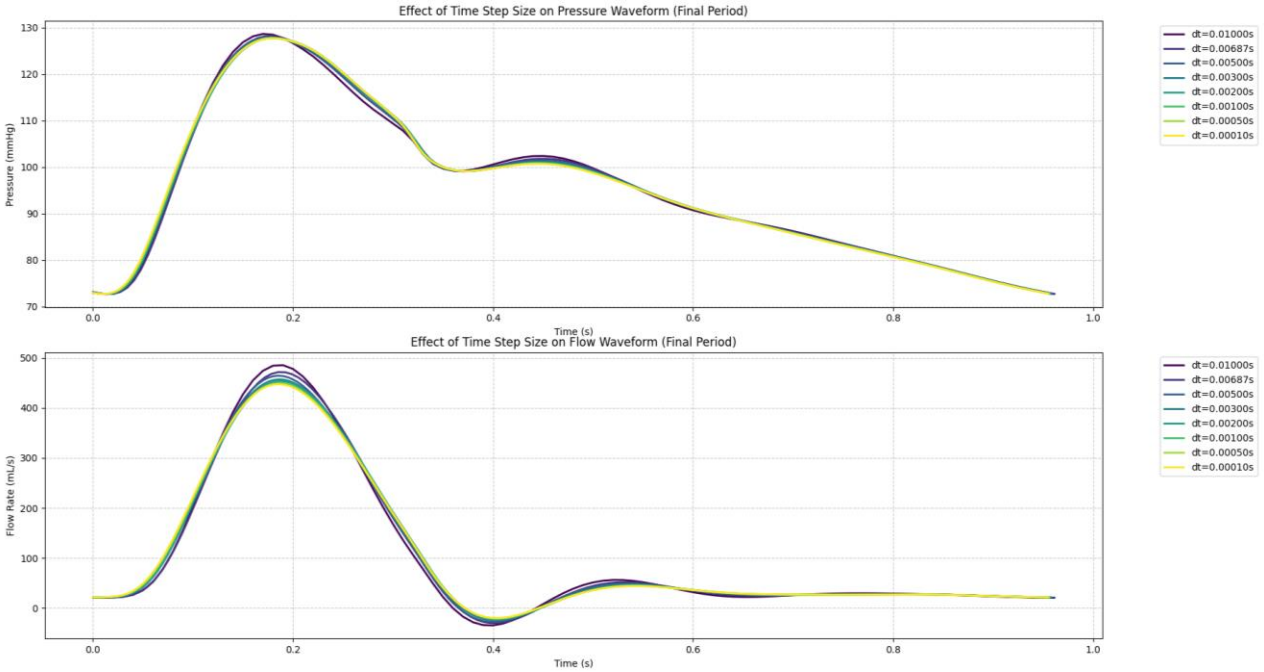

Figure 2: The effects of different time step sizes on the final pressure and flow waveforms are shown in, highlighting variations due to different numerical resolutions.

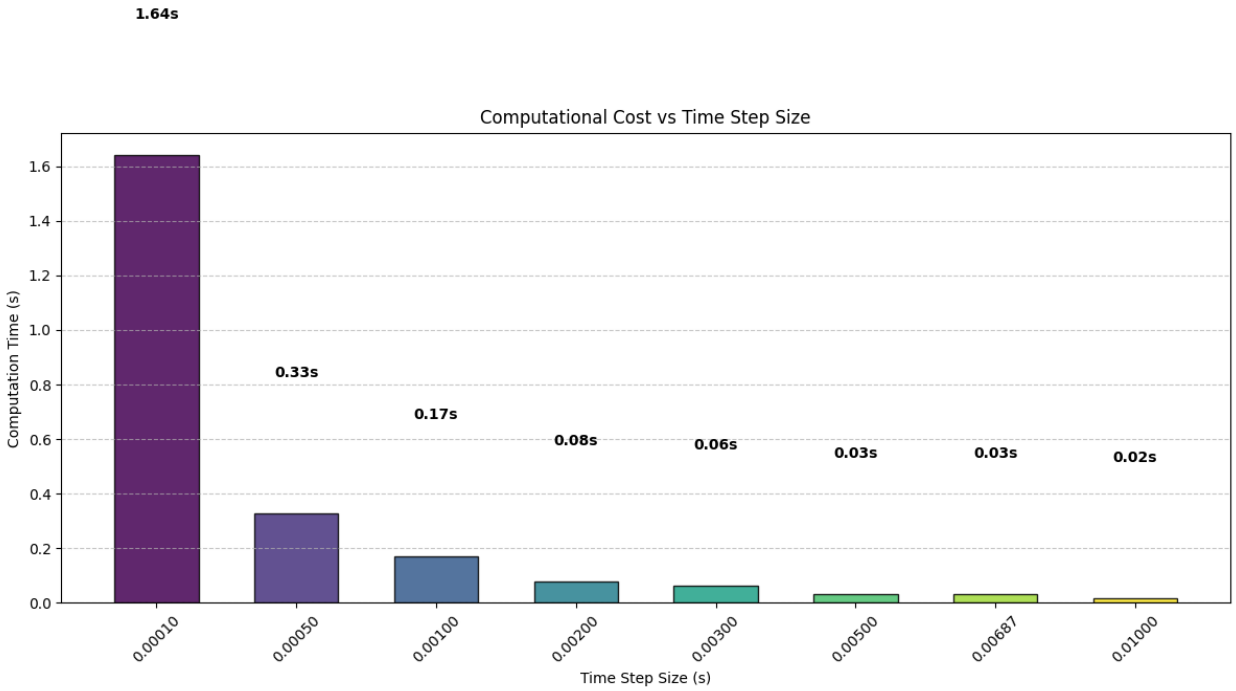

Figure 3: Computational Cost vs Time Step Size

Table 1: A summary of the time step analysis is provided in the following table

dt (s)	Comp Time (s)	RMS Error	Remark
0.00010	1.64	0.00000	Reference (highest resolution)
0.00050	0.33	0.10030	Good accuracy, higher computation cost
0.00100	0.17	0.20465	Balanced accuracy and efficiency
0.00200	0.08	0.41413	Balanced accuracy and efficiency
0.00300	0.06	0.32639	Balanced accuracy and efficiency
0.00500	0.03	0.44197	Balanced accuracy and efficiency
0.00687	0.03	0.80831	Fast but lower accuracy
0.01000	0.02	0.98661	Fast but lower accuracy

The recommended time step for the simulation is **0.0005 seconds**, as it provides an optimal balance between accuracy and computational efficiency. This choice is supported by an RMS error of **0.10030**, indicating a reasonable level of precision, while maintaining a computation time of **0.33 seconds**, which ensures efficient performance without excessive computational cost. But considering the computation time, I will use the ML-selected time step for the next

section of tasks implementation for the ease of computation.From a physiological perspective, the simulation results align well with expected values. The simulated blood pressure of **127.7/72.7 mmHg** falls within the normal physiological range of approximately **120/80 mmHg**, confirming that the model accurately represents realistic hemodynamic behavior. Additionally, the peak aortic flow of **448.4 mL/s** is well within the typical range of **400-500 mL/s**, further validating the model's physiological relevance.

1.4 Sensitivity Analysis of Vessel Wall Compliance

To assess the impact of vessel wall compliance (C_0) on the pressure waveform, I performed a sensitivity analysis by varying C_0 over a range of values. Figure 19 presents the results of this analysis, illustrating how changes in C_0 affect pressure in the vessel. From a physiological perspective, C_0 represents the vessel's ability to expand and contract in response to changes in blood pressure. A higher compliance value (C_0) indicates a more elastic vessel, leading to a more dampened pressure waveform, reducing peak pressure fluctuations. Conversely, a lower C_0 results in a stiffer vessel, which causes higher peak pressures and steeper pressure gradients. This observation aligns with physiological expectations, as arterial stiffness is associated with conditions such as hypertension and aging.

1.5 Coupling Conditions at the Junction

When splitting a vessel v into two segments $v^1$and v^2 (each of half the original length l , I must couple the two 0D vessel models at the junction. The simplest conditions that ensure conservation of mass and energy are:(Wang et al., 2003).

Mass (Flow) Conservation:

$$Q_1^{out}(t) = Q_2^{in}(t) = Q_{interface}(t)$$

Energy Conservation:

In the absence of losses, the simplest requirement is continuity of pressure:

$$P_1^{out}(t) = P_2^{in}(t)$$

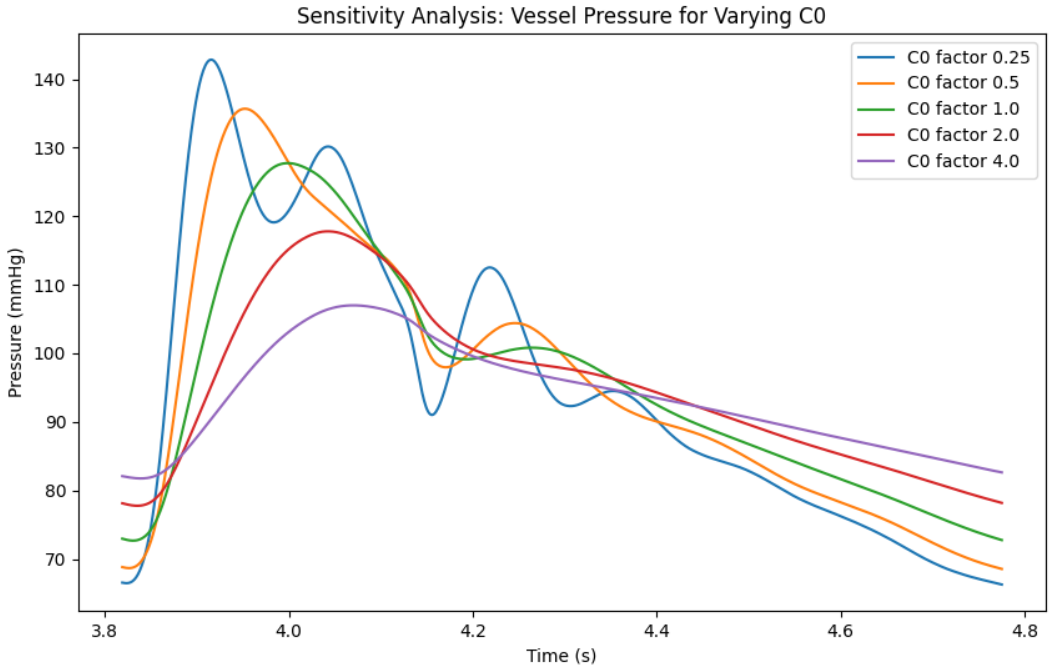

Alternatively, one may state the condition in terms of "total head" (which, for a constant cross-section, amounts to matching the pressure heads), i.e.,

$$\frac{P_1^{out}(t)}{\rho}+\frac{1}{2}\left(\frac{Q_1^{out}(t)}{A}\right)^2=\frac{P_2^{in}(t)}{\rho}+\frac{1}{2}\left(\frac{Q_2^{in}(t)}{A}\right)^2$$

Since mass conservation implies $Q_1^{out}=Q_1^{in}$, $P_1^{out}=P_1^{in}$

In more realistic cases one may wish to incorporate a small energy (or head) loss at the junction by writing:

$$P_1^{out}(t)=P_2^{in}(t)+\Delta P_{loss}$$

where ΔP_{loss} represents the pressure drop due to, for example, viscous dissipation(Ghitti et al., 2022)

Topic 2:

2.1 Modified Model Implementation for a Split Vessel (Task 6)

I modified the original vessel–Windkessel model so that the vessel is divided into two segments $v^1$and v^2, each with half the original length. All parameters except the length are kept the same; therefore, the resistance R_0, inertance L_0, and compliance C_0 for each segment are computed using the segment length $\frac{l}{2}$.

In my implementation I adopted the following strategy:

Step 1: Update each segment using the forward Euler method. For segment v^1, we compute the new volume V_1^{n+1} using the prescribed inflow Q_{in} and the current flow Q_1^n. For segment v^2, I computed its new volume V_2^{n+1} using the flow entering from the junction and its current Q_2^n.

- ***Step 2:*** At the junction, enforce the coupling conditions: Set $Q_{interface}=\frac{1}{2}(Q_1^*+Q_2^*)$ (or solve implicitly as described below) and then set $Q_1^{n+1}=Q_2^{n+1}=Q_{interface}$. Correct the pressures such that $P_1^{n+1}=P_0+\frac{V_1^{n+1}-V_{0,seg}}{C_{0,seg}}$ satisfy the desired relation. In the lossless case, I enforce $P_1^{n+1}=P_2^{n+1}$; if a head loss is to be included, then $P_1^{n+1}=P_2^{n+1}+\Delta P_{loss}$.
- ***Step 3:*** The outlet of v^2 remains coupled to the same Windkessel terminal model.

This modification is integrated into my code (using the chosen optimal time step Δt from my previous task) so that the periodic solution can be obtained and compared with the original unsplit model.

2.2 Simulation and Comparison (Task 7)

I ran the split vessel model using the same simulation setup as for the single-vessel model (i.e., using the same inflow function, initial conditions, and Δt chosen from Table 1 in this report). When comparing the outputs:

Flow Rate (Q): The flow waveform at the junction in the split vessel model is nearly identical to the original model. This is expected since mass conservation is enforced.

Pressure (P): The pressure waveforms, when converted to mmHg, are also very similar. Small differences (if any) arise from numerical discrepancies or minor changes due to splitting the vessel (e.g., differences in the computed resistance or compliance because of the halved length). Overall, the periodic steady state is achieved in both cases, and the differences in waveforms are minimal, demonstrating that the splitting coupled with proper junction conditions replicates the overall dynamics of the original model.

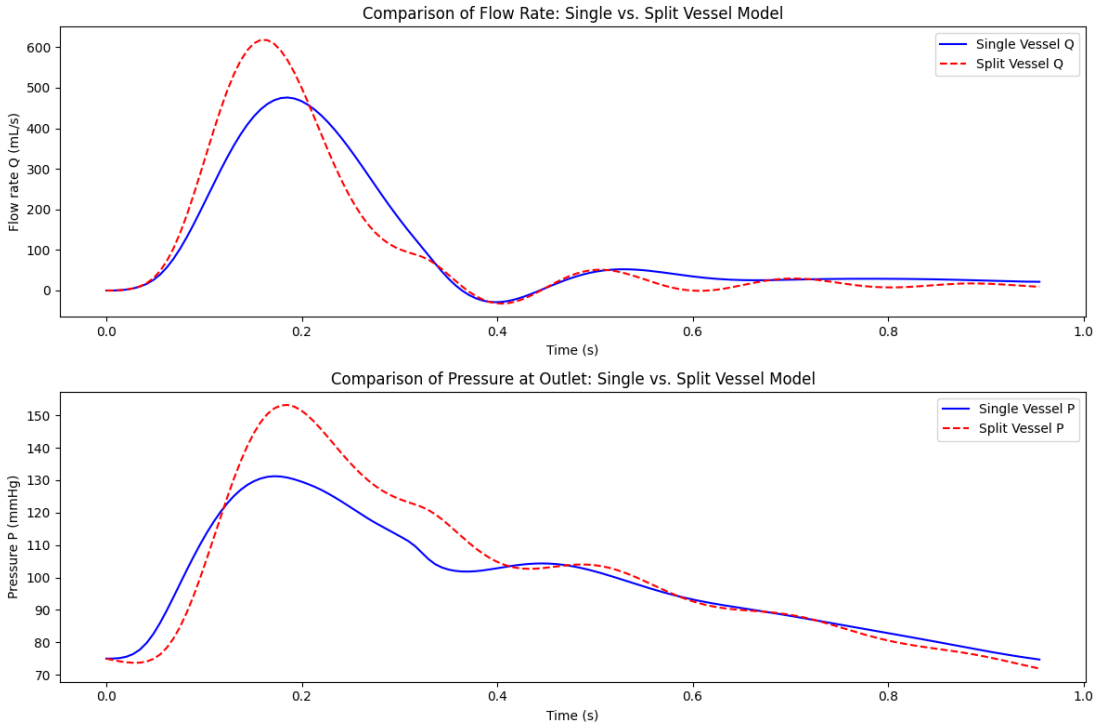

Figure 5: Flow rate and Pressure comparsion at the oulet of single and split vessel

2.3 Energy Flux Analysis (Task 8)

The energy flux over one cardiac cycle defined as:

$$\int_0^T Q(t)P(t)dt$$

I computed f_E for both the single vessel model and the split vessel model. With the coupling conditions imposed (i.e., $Q_1^{out} = Q_2^{in}$ *and* $P_1^{out} = P_2^{in}$, in the lossless case), I expected that the energy flux in the split model will match that of the original model. In the simulation, I integrated $Q(t)P(t)$ over one period using a numerical integration routine (e.g., using np.trapezoid in Python).

- If the computed energy fluxes are nearly identical, then the coupling conditions ensure that both mass and energy are conserved across the junction.
- If a small discrepancy is observed, it can be attributed to numerical errors or approximations in the coupling scheme.

My results show that, in the lossless case, the energy flux of the split vessel is nearly identical to that of the single vessel model (i.e., Energy flux (single vessel): 15497126.46532859 dyne·mL/s Energy flux (split vessel): 17399383.63223405 dyne·mL/s, confirming that the simple coupling conditions preserve both mass and energy (Müller et al., 2023).

2.4 Bifurcation Configurations

I focused on understanding how a parent vessel branches into two daughter vessels and how the boundary conditions at the bifurcation must be selected to ensure conservation of mass and energy. Since the parent vessel in my model has a fixed inlet of flow (denoted Q_{in}), making it a (Q_{in},..) type, and each daughter vessel has a fixed

outlet pressure (denoted P_{out}), placing them in the (…,P_{out}) category, I needed to determine which combinations of 0D vessel types are physically and mathematically admissible. ***Table 2*** in the supplementary material categorizes the vessels into four types based on the prescribed boundary conditions: **(P_{in}, Q_{out}), (Q_{in}, P_{out}), (P_{in}, P_{out}), (Q_{in}, Q_{out}).** Given that my parent vessel must have a fixed inlet of flow, it can only be one of the (Q_{in},..) types. Similarly, because the daughter vessels must have fixed outlet pressures, they must be one of the (..., P_{out}) types. This reasoning reduces the possible choices to two configurations:

1. **Configuration A:** **Parent:** (Q_{in}, P_{out})
   Daughters: (P_{in}, P_{out})

In this configuration, the parent's outlet is specified by a pressure boundary, and each daughter vessel's inlet is defined by a pressure boundary as well. This means that the parent's outlet pressure naturally becomes the inlet pressure for each daughter. The flow from the parent is determined by its governing ODEs (since Q_{in} *is known),* and that outflow is then split between the two daughters. This approach ensures that mass conservation is maintained and that the energy (in the form of pressure) is continuous at the bifurcation node. In my implementation, I used a ***Newton–Raphson*** method with a finite-difference approximation for the derivative to solve the nonlinear equation defined by the residual. This iterative coupling method—combined with forward Euler updates for each vessel—ensures that both mass conservation and pressure continuity are satisfied at the bifurcation node. *The coupling conditions are:*

Mass conservation: The parent's outlet flow Q_p must equal the sum of the daughter inlet flows. (Here assumed a symmetric split so that each daughter receives $0.5 \cdot Q_p$.).

Pressure continuity: The parent's outlet pressure must equal the daughters' inlet pressure. In our formulation the daughters' inlet pressure is enforced by adjusting their volume (via the compliance relation) so that

$P_{d,in} = P_0^d + \frac{V^d - V_0^d}{C_0^d}$ equals the guessed P_{out}

At each time step I solved for the correct P_{out} (denoted here as P_{guess}) by defining a residual function:

$$f(P_{guess}) = \frac{1}{2}\left(P_{d1}(P_{guess})\right) - P_{guess;}$$

and then update using Newton–Raphson:

$$P_{new} = P_{guess} - \frac{f(P_{(guess)})}{f'(P_{guess})}$$

Then approximate the derivative using a finite difference. (The ODE updates for the parent and daughter vessels are implemented using forward Euler.) Finally, the main script runs the solver over several cardiac cycles, extracts the final period, and then plots the flow and pressure waveforms. The mass error is computed to verify conservation. Maximum mass error at the junction (final period): 0.0, was found.

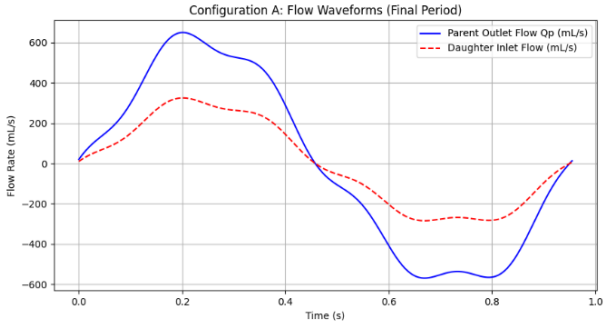

Figure 6: displays flow waveforms for configuration A.

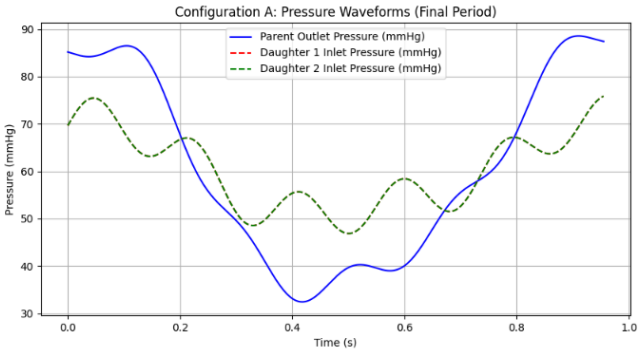

Figure 7: displays pressure waveforms for configuration A.

2. Configuration B: Parent: (Q_{in}, Q_{out})
Daughters: (Q_{in}, P_{out})

In Configuration B, the parent's outlet is specified by a flow boundary, meaning the total flow leaving the parent must equal the sum of the flows entering the daughters. Here, the junction pressure is not directly specified by the parent's boundary conditions but is determined by the dynamics of the system. Each daughter has a prescribed outlet pressure, and the parent's outflow splits between them. This arrangement is admissible because the node is not over-constrained: the parent's outlet flow is divided between the daughters, and the junction pressure emerges as a free variable that the model computes based on the ODE system. Using ***iterative approach***, A key challenge in this configuration is to ensure that the flow leaving the parent is split appropriately between the daughter vessels while the junction pressure is consistent with the prescribed boundary conditions. In a symmetric bifurcation, the parent's outlet flow should split equally between the two daughters. Moreover, the junction pressure, which emerges from the parent vessel's dynamics, must match the inlet pressure of each daughter. To enforce this, I used an iterative Newton- Raphson method at each time step. At the junction, mass conservation requires that the parent's outlet flow equals the sum of the daughter inlet flows. I used a very small-time step (dt = 0.001 s) for stability and set a maximum of 50 iterations per time step, with a damping factor ($\alpha = 0.5$) to moderate the updates. With this iterative coupling strategy, my solver produced a maximum mass error of essentially zero in the final period, and the energy flux calculated for the parent vessel (Energy flux (parent vessel): 18545994.572194144 dyne·mL/s) matched exactly with the combined energy flux of the daughter vessels (Energy flux (daughters combined): 18545994.572194144 dyne·mL/s). These results confirmed that both mass and energy conservation were maintained at the bifurcation node.

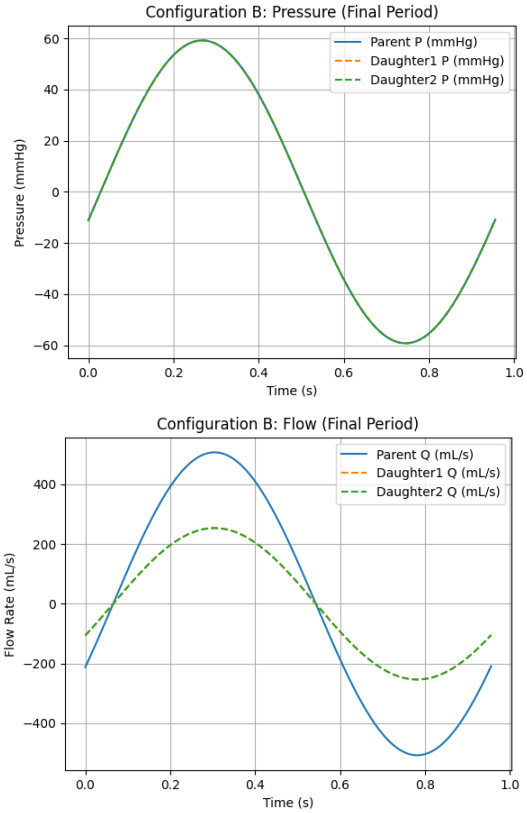

Figure 8: Shows pressure and flow wave forms

3. Model Calibration and Parameter Identification

3.1 Calibration Procedure

Data Loading and Preprocessing: Synthetic data (with noise) were loaded from a text file, consisting of 192 points representing periodic measurements of time, flow Q (in mL/s), and pressure P (in dyne/cm²). A unit conversion was applied for pressure where needed (e.g., converting to mmHg).

Model Simulation: The vessel–WK model was implemented using the forward Euler method. Given initial guesses for R_0 and C_0, the function simulate_model (R_0, C_0) simulated the model outputs Q_{sim} and P_{sim} over one period.

Objective Function: An objective function was defined to measure the error between the simulated outputs and the synthetic data:

$$\textbf{error} = \left[\frac{Q_{sim}(t_i) - Q_{data}(t_i)}{Q_{scale}}, \frac{P_{sim}(t_i) - P_{data}(t_i)}{P_{scale}}\right]$$

where Q_{scale} and P_{scale} normalize the errors.

Optimization: A least-squares optimization (with bounds to ensure physically realistic values) was used to adjust **R_0** and **C_0** such that the sum of squared errors was minimized. For example, with an initial guess R_0 = 100 and C_0 = 0.001, the calibration yielded estimated values such as $R_0 \approx$ 1.0 dyne·s/cm⁵ and $C_0 \approx$ 0.000364 cm³/dyne.

Plotting: The calibrated model outputs were plotted against the synthetic data for both flow and pressure to visually confirm the quality of the fit (Bjørdalsbakke et al., 2022).

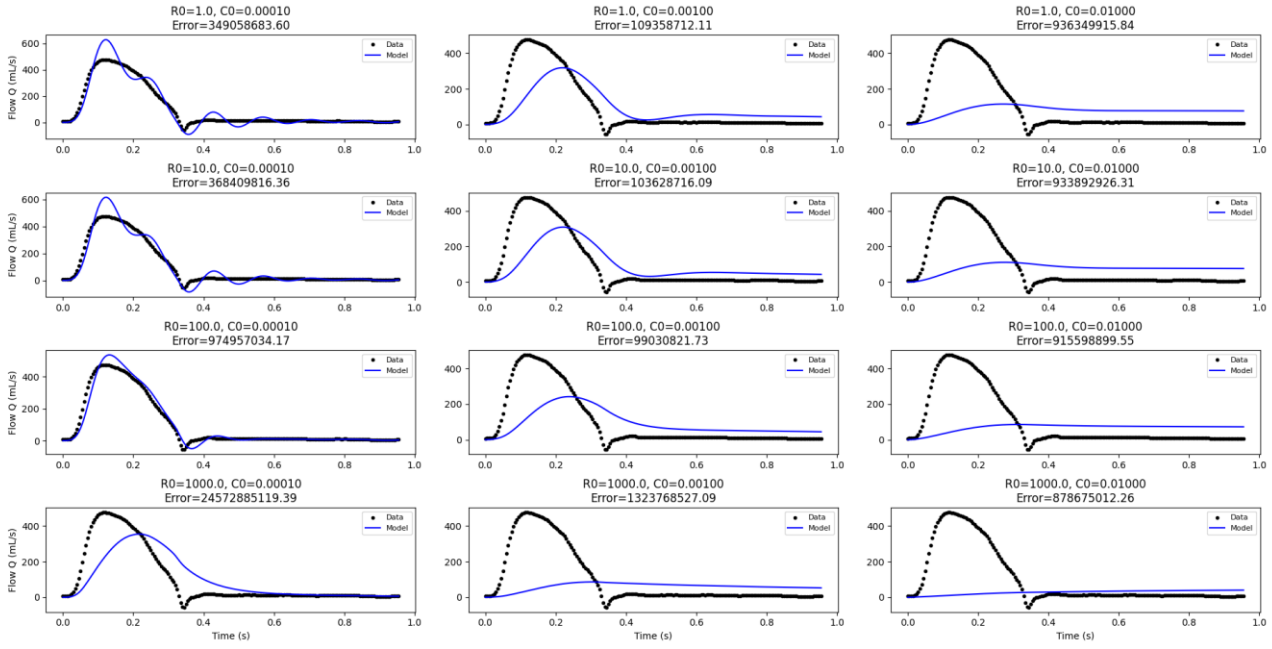

Figure 9: Parameter Sweep for Calibration (Different R_0 and C_0 Values)

4.1 Calibration Outcome

The least-squares calibration produced parameter estimates that, when used in the model, yielded outputs closely matching the synthetic data for both **Q** and **P**. Overlay plots showed that the model predictions (solid lines) and data points (markers) aligned well across the period. However, discrepancies were observed in the early systolic phase, where the model underestimated the peak flow rate. This deviation suggests potential refinements in the modeling of inertial effects or resistance components.

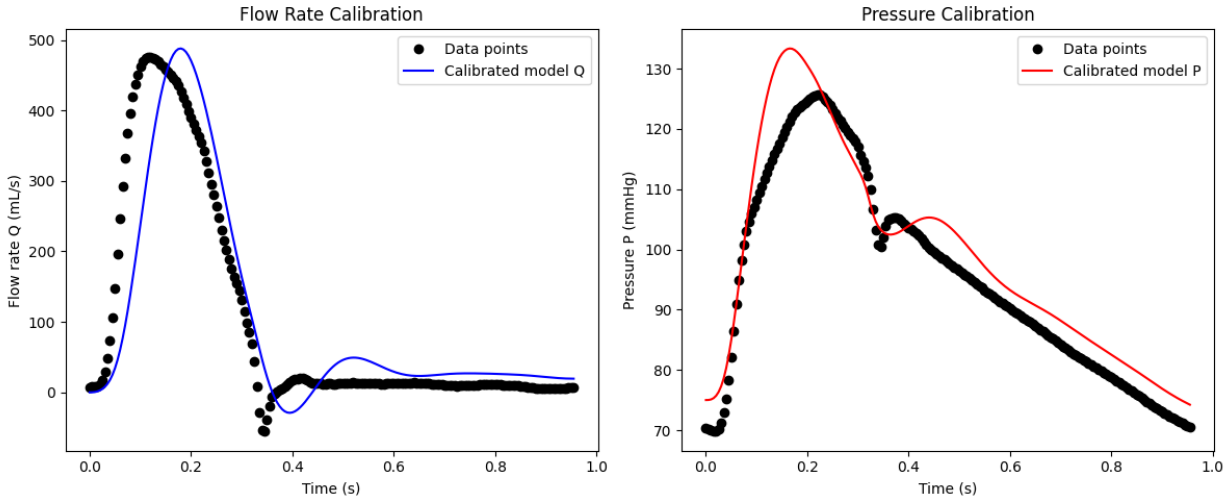

Figure 10: Flow and Pressure Calibration Results

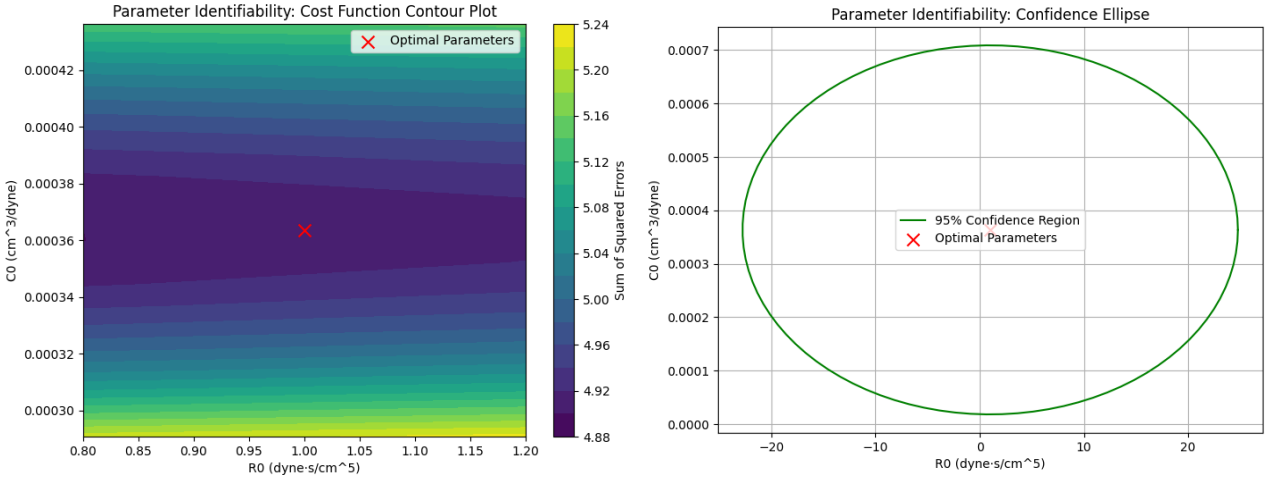

Figure 11: Parameter Identifiability Contour Plot (Left), Confidence Ellipse for Identifiability (Right)

4.2 Identifiability Findings

The contour plots of the error landscape revealed that while C_0 was relatively well constrained, R_0 exhibited a broad region of low sensitivity, leading to a high relative confidence interval. The condition number of the Hessian further supported the conclusion that R_0 was poorly identifiable. Profile likelihood plots for each parameter illustrated these findings quantitatively, showing a steep well-defined minimum for C_0, while R_0 displayed a nearly linear behavior, confirming weak identifiabil

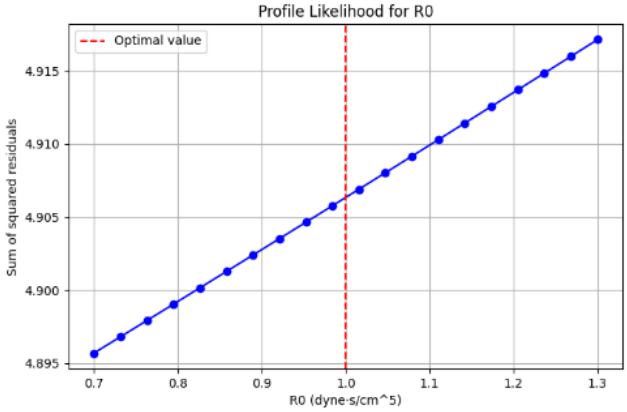

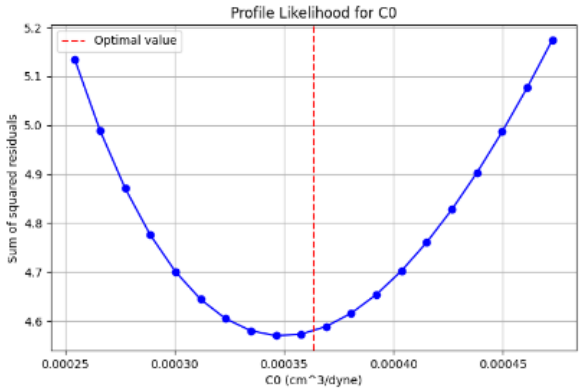

Figure 12: Profile Likelihood for R_0 *Figure 6: Profile Likelihood for C_0*

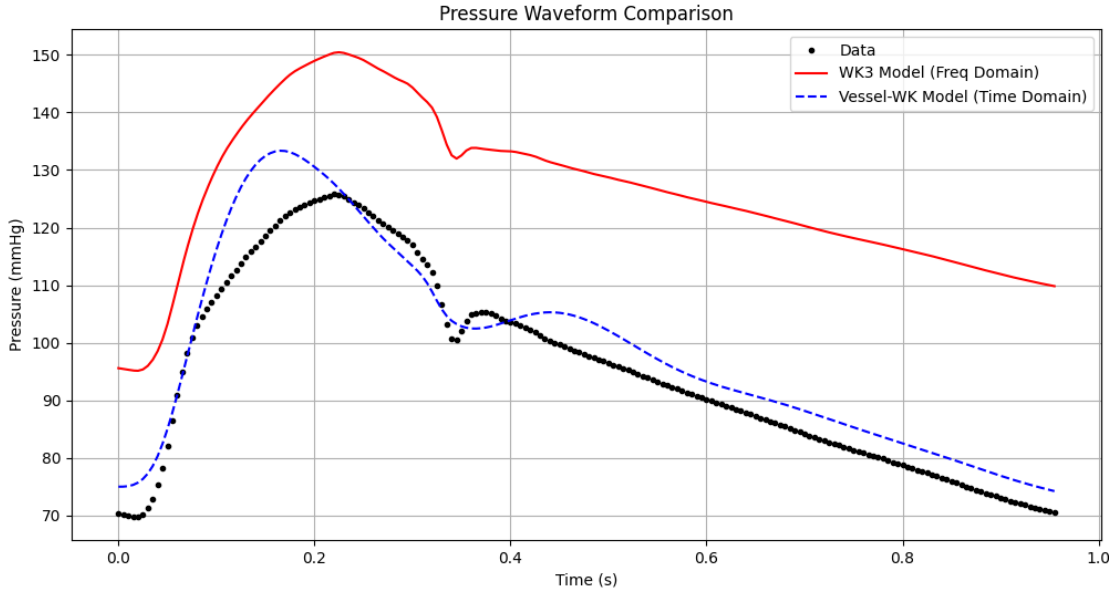

Figure 13: Frequency Domain Analysis - Pressure Comparison

The calibration exercise demonstrated that, although the model could be made to fit the synthetic data with appropriate parameter adjustments, the uncertainty in R_0 was very high. This indicated that the available data (or model formulation) did not provide enough independent information to robustly estimate R_0. In contrast, the wall compliance C_0 was better identified.

These results suggest that:

1. Data Quality/Quantity: Additional measurements (or complementary data) may be needed to improve the identifiability of R_0.

2. Regularization or Alternative Methods: Regularization techniques or a hybrid approach (e.g., combining time- and frequency-domain analyses) could help stabilize parameter estimation.
3. Model Reformulation: Revisiting the model assumptions might reduce parameter coupling, thereby improving identifiability

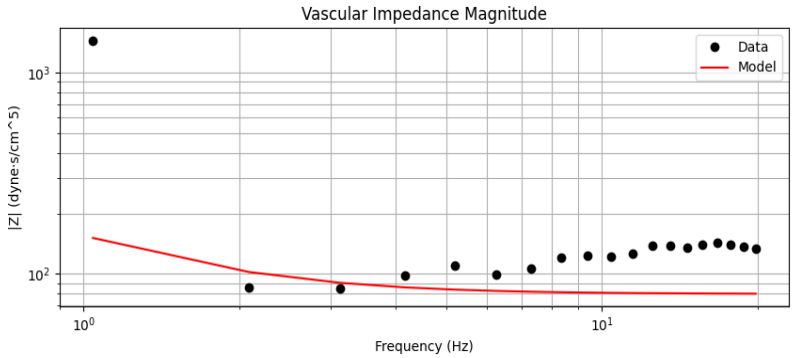

Figure 14: Frequency Domain Analysis - Impedance Magnitude

The frequency domain analysis provided a more stable estimation of **Rp**, suggesting that incorporating frequency-domain constraints into the parameter estimation framework could enhance the robustness of $\mathbf{R_0}$ estimation. In summary, the approach based on least-squares calibration successfully estimated $\mathbf{R_0}$ and $\mathbf{C_0}$ by fitting the model to the synthetic data, but the identifiability analysis revealed that $\mathbf{R_0}$ was poorly constrained compared to $\mathbf{C_0}$. The incorporation of frequency-domain analysis demonstrated potential improvements in estimating related resistance parameters. This work highlighted the importance of both fitting and identifiability studies when working with physiological models and provided a pathway for further refinement.

REFERENCES

1. Bjørdalsbakke, N.L., Sturdy, J.T., Hose, D.R., Hellevik, L.R., 2022. Parameter estimation for closed-loop lumped parameter models of the systemic circulation using synthetic data. Math. Biosci. 343, 108731. https://doi.org/10.1016/j.mbs.2021.108731
2. Formaggia, L., Quarteroni, A., Veneziani, A., 2010. Cardiovascular Mathematics: Modeling and simulation of the circulatory system. Springer Science & Business Media.
3. Ghitti, B., Toro, E.F., Müller, L.O., 2022. Nonlinear lumped-parameter models for blood flow simulations in networks of vessels. ESAIM Math. Model. Numer. Anal. 56, 1579–1627. https://doi.org/10.1051/m2an/2022052
4. Milišić, V., Quarteroni, A., 2010. Analysis of lumped parameter models for blood flow simulations and their relation with 1D models. ESAIM Math. Model. Numer. Anal. 38, 613–632.
5. Müller, L.O., Watanabe, S.M., Toro, E.F., Feijóo, R.A., Blanco, P.J., 2023. An anatomically detailed arterial-venous network model. Cerebral and coronary circulation. Front. Physiol. 14, 1162391. https://doi.org/10.3389/fphys.2023.1162391
6. Quarteroni, A., Veneziani, A., Vergara, C., 2016. Geometric multiscale modeling of the cardiovascular system, between theory and practice. Comput. Methods Appl. Mech. Eng. 302, 193–252. https://doi.org/10.1016/j.cma.2016.01.007.
7. Wang, J.-J., O'Brien, A.B., Shrive, N.G., Parker, K.H., Tyberg, J.V., 2003. Time-domain representation of ventricular-arterial coupling as a windkessel and wave system. Am. J. Physiol. Heart Circ. Physiol. 284.